Building small scales in MHD turbulence

A. Verdini*, R. Grappin†, R. Pinto** and M. Velli‡

*Solar-Terrestrial Center of Excellence - SIDC, Royal Observatory of Belgium, Bruxelles
†LUTH, Observatoire de Paris, CNRS, Université Paris-Diderot, and LPP, Ecole Polytechnique, Palaiseau
**Laboratoire AIM Paris-Saclay, CEA/Irfu, and Université Paris-Diderot CNRS/INSU, Gif-sur-Yvette, France
‡Dipartimento di fisica, Universitá di Firenze, Firenze, and JPL, Pasadena

Abstract. Magneto-hydrodynamic turbulence (MHD) with a mean large-scale field is known to produce an anisotropic cascade, with energy mostly in perpendicular scales. For strong turbulence small parallel scales are generated from the transport of perpendicular scales along the magnetic field, following the so called critical balance condition that predicts $E_{||}^{1D} \propto k_{||}^{-2}$. Weak turbulence is not expected to develop small parallel scales and to become strong at smaller perpendicular scales. We use a shell-model version of the Reduced MHD equations to simulate turbulence in homogeneous periodic conditions, in coronal loops, and in the solar wind. We compare the perpendicular and parallel spectra and show that different regimes of weak turbulence develop in loops and in the solar wind. We briefly comment on the way their characteristic large-scale features influence the weak turbulence spectra and their transition to strong turbulence.

Keywords: Magnetohydrodynamics (MHD) — plasmas — turbulence — solar wind
PACS: 47.65.-d, 47.27.Jv, 47.27.Gs

INTRODUCTION

Magneto-hydrodynamic turbulence with strong guiding field B_0 is known to develop an anisotropic spectrum with energy cascading mainly in the perpendicular scales. In the framework of Reduced MHD the cascade adopts two regimes, depending on the importance of the two timescales that rule the dynamics in the perpendicular and parallel directions at the largest scales, namely the eddy-turnover time $t_{NL}^0 = (k_\perp^0 b_{rms})^{-1}$ and the Alfvén timescale $t_A^0 = (k_{||}^0 V_A)^{-1}$. We define $k_\perp^0$ and $k_{||}^0$ as the large-scale perpendicular and parallel wavenumbers, $V_A = B_0/\sqrt{2\pi\rho}$ is the Alfvén speed along the mean magnetic field, and $b_{rms} = \delta b/\sqrt{2\pi\rho}$ is the fluctuations' amplitude in the large-scale eddies (written in velocity units).
For $t_A^0 < t_{NL}^0$ the perpendicular cascade is weak because the nonlinear transfer is interrupted by modulation in the parallel direction due to the propagation of Alfvén waves along the mean field, resulting in a 1D perpendicular spectrum $E_\perp^{1D} \propto k_\perp^{-2}$ [1], while parallel energy remains at scale $k_{||}^0$, with no small-scale formation. As the nonlinear timescale decreases with perpendicular wavenumber, t_{NL} becomes comparable to t_A^0 and the cascade switches to the strong regime. According to the critical balance conjecture [2] the two timescales maintain an equilibrium for higher $k_\perp$ with t_{NL} being ruled by the strong perpendicular cascade $b \propto k_\perp^{-1/3}$. Parallel scales are formed due to the advection along the mean field of the perpendicular structure, resulting in the relation $k_{||} \propto k_\perp^{2/3}$. The reduced parallel spectra follow the power laws $E_\perp^{1D} \propto k_\perp^{-5/3}$ and $E_{||}^{1D} \propto k_{||}^{-2}$ (if a scale-dependent alignment is at work [3] the perpendicular spectrum assumes the slope $3/2$ instead of $5/3$). For $t_A^0 > t_{NL}^0$ the cascade is strong already at the large scales, and the above scaling apply to the whole spectral range.

A version of RMHD build on Shell Models (Shell-RMHD or hybrid shell model) has been applied to study the contribution of turbulence in the heating of coronal loops [4, 5, 6], the heating and the acceleration of the solar wind [7, 8], and recently to characterize the transition from weak to strong turbulence in the periodic homogeneous case [9], in order to compare to direct numerical simulations of the RMHD equations [10]. We will revisit shortly the results obtained in the homogenous periodic case, in the applications to turbulence in coronal loop and in the solar wind. To this aim we will compare the characteristic timescales imposed by the forcing, as dictated by the problem at hand, with the timescales introduced by the large scale structure of coronal loops and coronal holes to understand which kind of turbulence regime develops (weak or strong) and which are its properties. In general the forcing term depends on three parameters, the correlation time of the forcing t_{cor}^f, the forced perpendicular wavenumber $k_\perp^f$, and the forced parallel wavenumbers $k_{||}^f$. The last two define two additional timescales, the eddy turnover time at forced scales $t_{NL}^f = (k_\perp^f z_{rms})^{-1}$ and the Alfvén time at forced scales $t_A^f = (k_{||}^f V_a)^{-1}$. The latter has a meaning only for the periodic-homogenous case, where we use volume forcing. When studying coro-

nal loops and coronal holes we will use a surface forcing applied at one boundary only.

HOMOGENEOUS PERIODIC TURBULENCE

The RMHD equations are written in the mixed Fourier-Real space (x, k_y, k_z). The nonlinear convolutions in (k_y, k_z) are then replaced by the lighter subset of 2D shell models [11], each plane is connected to the others by the parallel propagation of Alfvén waves, followed in the real space. The equations for the Elsasser variables $z_n^{\pm}(x,t) \equiv z^{\pm}(x,k_n,t)$ read:

$$\partial_t z_n^{\pm} \pm V_a \partial_x z_n^{\pm} = i T_{npq}^{\pm} - \nu k_n^2 z_n^{\pm} + f_n^{\pm} \qquad (1)$$

where $k_n = k_0 2^n$ is the perpendicular wavenumber associated to each mode $z_n^{\pm}$, and $T_{npq}^{\pm}$ stands for the nonlinear interactions in the shell model. The forcing terms $f_n^{\pm}$ represent a volume forcing applied on the velocity fluctuations only ($f^{\pm} = f^u$) at large perpendicular scales $n = 0, 1, 2$, thus the timescales for the two species $z^{\pm}$ are the same and we will omit to specify the label $\pm$. We fix $B_0 \equiv V_a = 5$, the aspect ratio $L_{\perp}/L_{||} = 1/5$, and tune the forcing so that $b_{rms} \approx 1$. In this homogeneous periodic case the volume forcing defines completely the Alfvén and the nonlinear timescales at large scales ($t_A^f \equiv t_A^0$, $t_{NL}^f \equiv t_{NL}^0$). For simplicity the correlation time of the forcing will be adapted so that $t_{cor}^f = t_A^f$ and we will vary the excited parallel scales in order to drive turbulence in the weak or strong regime: (i) in the strong-forcing case we excite the parallel mode equal to 1, $k_{||}^f = k_{||}^0$, at forcing scales the critical balance condition $t_A^0 \approx t_{NL}^0$ is satisfied and the strong regime holds from start. (ii) in the weak-forcing case we excite the parallel modes from 1 to 16, at forcing scales turbulence is in the weak regime $t_A^0 < t_{NL}^0$.

The 1D reduced perpendicular and parallel spectra are plotted in fig. 1 for the two cases. In the strong forcing case the perpendicular spectrum has a power law with index around $-5/3$ and in the weak forcing case the slope switches from -2 to $-5/3$ when the cascade passes from the weak regime, imposed by the driving, to the critically-balanced strong regime at higher wavenumbers. This switch actually corresponds to the transition from $t_A \approx t_A^0$ to $t_A \approx t_{NL}$ [9] as predicted by the Goldreich and Sridhar [2] phenomenology. Despite this basic agreement, the reduced parallel spectra does not follow the CB prediction $E_{||}^{1D} \propto k_{||}^{-2}$ (red line in the right panel). Instead the scaling is $-5/3$ for the strong forcing case, and arounf -3 for the weak-forcing case beyond the forced scales (where peaks in the parallel spectrum appear).

In this periodic homogeneous case the parallel spectrum and the frequency spectrum are identical, and are related by $k_{||} = \omega/V_A$. In the following we will consider cases in which the parallel spectrum is difficult to measure because the configurations are no more periodic: we will compare the frequency spectrum with the above parallel spectrum without any further warning.

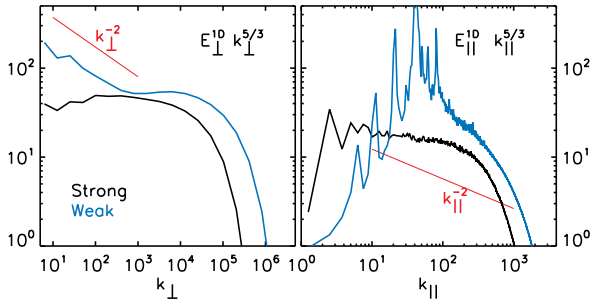

FIGURE 1. Compensated 1D (reduced) perpendicular spectrum (left) and parallel spectrum (right) for the case of strong and weak forcing (black and blue lines respectively) for turbulence in the homogenous periodic case.

TURBULENCE IN CORONAL LOOPS

In order to describe turbulence in coronal loops we replace the periodic boundary condition with semi-reflecting boundary conditions mimicking the effect of the density jump occurring at the transition region. We have two important modifications with respect to the homogeneous case. First, the coronal loop behaves as a resonant cavity, supporting resonant modes with well-defined frequencies $\omega^{res} = m/t_A^c$ and wavenumbers $k_{||}^{res} = m/L^c$ (with $m = 0, 1, 2..$), where $t_A^c = L^c/V_A^c$ is the coronal crossing time and L^c the length of the loop. Second, the cavity is not perfect, since the density jump is finite, and some energy leaks out through the transition region on the long leakage timescale $t_L = t_A^c/\varepsilon$, where $\varepsilon \approx 10^{-2}$ is the square root of the density jump across the transition region [12, 8]. The strong reflection at the transition regions assures $z^+ \approx z^-$ and we will omit the label $\pm$ when referring to timescales. The forcing is now applied at the coronal boundaries of the loop (surface forcing) in order to mimic the effect of photospheric footpoint motions that inject Alfvén waves inside the loop. We chose $t_{cor}^f = \infty$ (constant forcing, a more accurate condition would be $t_{cor}^f >> t_A^c$), we fix the amplitude $z^f = 1$. In practice we will have the following ordering by construction $t_{cor}^f >> t_L >> t_A^c$ and we will change the injection perpendicular scale $k_{\perp}^f$ in order to drive a weak turbulence regime ($t_A^c < t_{NL}^f$) or a strong regime ($t_A^c > t_{NL}^f$). When driving in the weak regime we will keep $t_{NL}^f < t_L$, if it is not the case energy leaks out from the

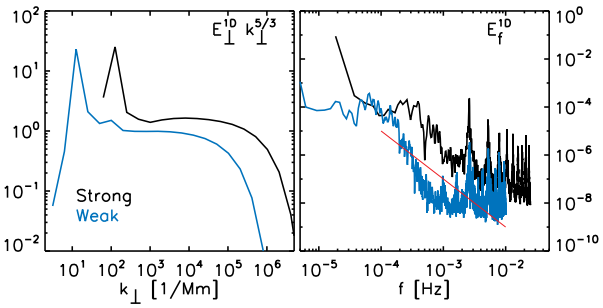

FIGURE 2. Compensated 1D (reduced) perpendicular spectrum (left) and frequency spectrum (right) for the case of of strong and weak forcing (black and blue lines respectively) for turbulence in coronal loops.

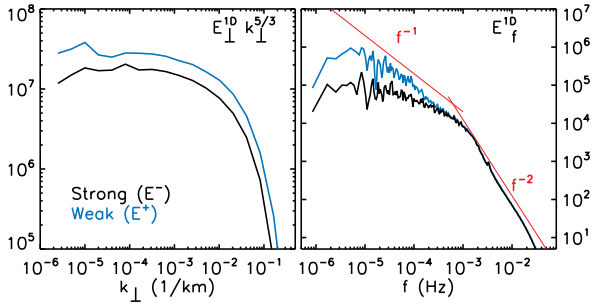

FIGURE 3. Compensated 1D (reduced) perpendicular spectrum (left) and frequency spectrum (right) for solar wind turbulence at a distance of 19 $R_\odot$, just outside the Alfvénic critical point. Weak and strong refers to the cascade of the two species ($z^\pm$) and not the the forcing.

corona without producing any turbulent dynamics. Note that we implicitly assumed that t_A^c plays the role of the Alfvén timescale in the homogenous periodic case, in other words the fluctuations acquire a short Alfvén time, inherited from the resonant behavior of loops, that may weaken the cascade.

In the left panel of fig. 2 we plot the compensated perpendicular spectra. In both weak and strong driving there is a bump at small wavenumber followed by an inertial range with slope $-5/3$ that extends for a few decades. Independently of the driving, turbulence develops a weak regime that is not characterized by a power law spectrum. The presence of resonances is clearly seen in the right panel where the frequency spectrum is plotted. Energy is mainly accumulated in the first resonance ($\omega^{res}=0$, corresponding to magnetic energy accumulation) in both cases. For weak driving the spectrum falls off abruptly at $f\approx 1/t_L$ and then higher resonances are excited emerging from an overall flat spectrum. High frequency resonances ($\omega^{res}=1/t_A^c,\ 2/t_A^c...$) are energetically important, weakening the nonlinear interactions [13, 14]: the leakage towards the chromosphere is the primary energy loss that balances the accumulation of coronal energy (the energy in the bump visible in the perpendicular spectrum). For strong driving the spectrum follows approximately an f^{-2} scaling (red line), as expected from critical balance, over which the excited resonances emerge. They still play a role in weakening the perpendicular cascade (the bump at low $k_\perp$ is still present), but the turbulent cascade contribute also to the losses that limit the energy accumulation, leading to strong heating.

Note that in simulations of the full RMHD equations the bump is not seen, and the weak turbulent regime produces a power-law spectrum whose slope increases with the strength of the axial magnetic field, i.e. the weaker the turbulence the steeper the spectra [15, 16]. This may be due to the lower Reynolds number achievable in DNS, but also to the richer nonlinear dynamics of the full RMHD equations compared to the Shell-RMHD.

TURBULENCE IN THE SUB-ALFVÉNIC SOLAR WIND

To describe turbulence in the sub-Alfvénic solar wind we consider the geometry of a coronal hole that expands super-radially and in which the density decreases with height by several order of magnitude under the solar wind expansion. The Shell-RMHD equations (1) contain additional terms accounting for the stratification (ρ), the presence of the solar wind (U), and the super-radial expansion (A):

$$\partial_t z_n^\pm + (U\pm V_a)\partial_x z_n^\pm - \frac{1}{4}(U\mp V_a)\left(\frac{1}{\rho}\frac{d\rho}{dx}\right) z_n^\pm + \frac{1}{4}(U\mp V_a)\left(\frac{1}{\rho}\frac{d\rho}{dx} - 2\frac{1}{A}\frac{dA}{dx}\right) z_n^\mp = T_{npq}^\pm - \nu k_n^2 z^\pm \qquad (2)$$

The density stratification and the solar wind expansion introduces major differences. At variance with the coronal loop case there is only one transition region here, causing strong reflection and thus $z^-\approx z^+$ in the chromosphere. However the density scale height in the corona increases, reflection is weaker and $z^-\approx 1/10\ z^+$ in the corona and in the solar wind. This implies $t_{NL}^+ > t_{NL}^-$. Moreover, the Alfvénic critical point $X_A\approx 15R_\odot$ represents an escape point for waves: beyond X_A the wind speed overcomes the Alfvén speed advecting the fluctuations in the heliosphere. Expansion affects the strength of turbulence since the perpendicular wavenumbers decrease with distance as $k_\perp = k_\perp^\odot R_\odot/R$. The forcing is defined in a similar way as in coronal loops, it has the characteristic correlation time $t_{cor}^f\approx 600$ s of the photospheric motions and an eddy-turnover time $t_{NL}^f = (k_\perp^f z_f^+)^{-1}\approx$ 540 s, with $k_\perp^f\approx 2\pi/34$ Mm representing the size of su-

pergranulation, and $z_f^+ = 10$ km/s is the amplitude of the fluctuations entering the chromosphere. In practice the forcing fixes two timescales at the lower boundary: the correlation time $t_{cor}^+ \approx t_{cor}^f$ for the outward propagating wave and the eddy turnover time $t_{NL}^- \approx t_{NL}^f$ for the inward propagating (reflected) wave. The other timescales t_{cor}^- and t_{NL}^+ are given by turbulent dynamics inside the coronal hole, and are affected by reflection and the different propagation speeds of $z^\pm$. In particular one finds that with the above forcing, z^- is subject to a strong cascade, while z^+ undergoes a weak cascade [8].

In figure 3 we plot the compensated perpendicular spectra and the frequency spectra for the two species at the distance of 19 $R_\odot$, well above the Alfvénic critical point. The perpendicular spectra resemble each other, despite the different turbulent regimes, showing an approximate inertial range with slope 5/3. This is caused by the reflection of z^- at the transition region, that brings its well developed spectrum into the weakly cascading z^+. The frequency spectra have a high frequency tail with slope f^{-2}, consistent with the critical balance prediction. At low frequencies the dominant z^+ takes a $1/f$ slope caused by the combined effect of reflection and weak cascade.

CONCLUDING REMARKS

We have shown that (i) the transition from weak to strong cascade is captured for the first time using RMHD equations implemented with shell models. This transition agrees with the critical balance prediction, in term of perpendicular spectra and timescales, but the parallel spectra do not follow the predicted $k_\parallel^{-2}$ slope, showing instead an excitation of small parallel scales with slope $-5/3$ in the case of strong turbulence. (ii) weak turbulence develops in coronal loops and in coronal holes, because of the characteristic timescales of the driving (photospheric footpoint motions) and because of their large scale density structure. Parallel spectra differ in all three cases, showing a variety of spectral slopes that bring the imprints of the structure in which turbulence develops.

We stress that the cascade rate is influenced by such features. While in the homogenous periodic case the cascade rate is the same for the weak and strong turbulence case, in coronal loops the cascade time is controlled by the kinetic energy in resonances (u_c). Although we are not able to predict u_c the expression $t_{casc} = l_\perp V_A^c / u_c^2$ perfectly fits the heating rate obtained in Shell-RMHD simulations as the ones presented above and depends on the large scale features of the loop, i.e. its width $l_\perp$, density and magnetic field. For the solar wind the situation is more complicated, we are currently working to understand the role of imbalance between the two Elsasser variables ($z^\pm$) and the simultaneous presence of a weak and a strong regime.

ACKNOWLEDGMENTS

A.V. acknowledges support from the Belgian Federal Science Policy Office through the ESA-PRODEX program.

REFERENCES

1. S. Galtier, S. V. Nazarenko, A. C. Newell, and A. Pouquet, *Journal of Plasma Physics* **63**, 447–488 (2000).
2. P. Goldreich, and S. Sridhar, *Astrophysical Journal* **438**, 763–775 (1995).
3. S. Boldyrev, *The Astrophysical Journal* **626**, L37–L40 (2005).
4. G. Nigro, F. Malara, V. Carbone, and P. Veltri, *Physical Review Letters* **92**, 194501 (2004).
5. E. Buchlin, and M. Velli, *The Astrophysical Journal* **662**, 701 (2007).
6. A. Verdini, R. Grappin, and M. Velli, *Astronomy & Astrophys.* **538**, A70 (2012).
7. A. Verdini, M. Velli, and E. Buchlin, *The Astrophysical Journal Letters* **700**, L39 (2009).
8. A. Verdini, R. Grappin, R. Pinto, and M. Velli, *The Astrophysical Journal Letters* **750**, L33 (2012).
9. A. Verdini, and R. Grappin, *Physical Review Letters* **109**, 25004 (2012).
10. J. C. Perez, and S. Boldyrev, *The Astrophysical Journal* **672**, L61–L64 (2008).
11. P. Giuliani, and V. Carbone, *Europhysics Letters* **43**, 527–532 (1998).
12. R. Grappin, G. Aulanier, and R. Pinto, *A&A* **490**, 353–356 (2008).
13. G. Nigro, F. Malara, and P. Veltri, *The Astrophysical Journal* **685**, 606 (2008).
14. F. Malara, G. Nigro, M. Onofri, and P. Veltri, *The Astrophysical Journal* **720**, 306 (2010).
15. P. Dmitruk, D. O. Gómez, and W. H. Matthaeus, *Physics of Plasmas* **10**, 3584–3591 (2003).
16. A. F. Rappazzo, M. Velli, G. Einaudi, and R. B. Dahlburg, *The Astrophysical Journal* **657**, L47–L51 (2007).